AGU ADVANCING EARTH AND SPACE SCIENCE

Geophysical Research Letters®

RESEARCH LETTER
10.1029/2022GL098511

Rainbow of the Night: First Direct Observation of a SAR Arc Evolving Into STEVE

C. Martinis[1], I. Griffin[2,3], B. Gallardo-Lacourt[4,5], J. Wroten[1], Y. Nishimura[6], J. Baumgardner[1], and D. J. Knudsen[7]

[1]Center for Space Physics, Astronomy Department, Boston University, Boston, MA, USA, [2]Citizen Scientist, Otago Museum, Dunedin, New Zealand, [3]Dodd-Walls Centre, Department of Physics, University of Otago, Dunedin, New Zealand, [4]NASA Goddard Space Flight Center, Greenbelt, MD, USA, [5]The Catholic University of America, Washington, DC, USA, [6]Center for Space Physics, Department of Electrical and Computer Engineering, BostonUniversity, Boston, MA, USA, [7]Department of Physics and Astronomy, University of Calgary, Calgary, Alberta, Canada

Key Points:

- Citizen scientist images show for the first time the evolution of a stable auroral red (SAR) arc into Strong Thermal Emission Velocity Enhancement (STEVE)
- An all-sky imager measured a bright, ~6 kR, SAR arc colocated with the arc observed by the citizen scientist when the emission height is 425 km
- Swarm data show subauroral ion drift conditions during a conjunction with the SAR arc observation. Later, these conditions intensify when STEVE is measured

Supporting Information:

Supporting Information may be found in the online version of this article.

Correspondence to:

C. Martinis,
martinis@bu.edu

Citation:

Martinis, C., Griffin, I., Gallardo-Lacourt, B., Wroten, J., Nishimura, Y., Baumgardner, J., & Knudsen, D. J. (2022). Rainbow of the night: First direct observation of a SAR arc evolving into STEVE. *Geophysical Research Letters*, *49*, e2022GL098511. https://doi.org/10.1029/2022GL098511

Received 28 FEB 2022
Accepted 2 MAY 2022

Author Contributions:

Conceptualization: C. Martinis, B. Gallardo-Lacourt
Data curation: I. Griffin, J. Wroten, D. J. Knudsen
Formal analysis: C. Martinis
Investigation: C. Martinis, B. Gallardo-Lacourt, Y. Nishimura
Methodology: C. Martinis, B. Gallardo-Lacourt
Resources: I. Griffin, J. Wroten, Y. Nishimura, J. Baumgardner, D. J. Knudsen
Validation: D. J. Knudsen
Visualization: C. Martinis, J. Wroten
Writing – original draft: C. Martinis
Writing – review & editing: C. Martinis, I. Griffin, B. Gallardo-Lacourt, J. Wroten, Y. Nishimura, J. Baumgardner, D. J. Knudsen

Abstract During the 17 March 2015 geomagnetic storm, citizen scientist observations from Dunedin (45.95°S, 170.32°E), New Zealand, revealed a bright wide red arc known as stable auroral red (SAR) arc evolving into a thin white-mauve arc, known as Strong Thermal Emission Velocity Enhancement (STEVE). An all-sky imager at the Mount John Observatory (43.99°S, 170.46°E), 200 km north of Dunedin, detected an extremely bright arc in 630.0 nm, with a peak of ~6 kR, colocated with the arc measured at Dunedin at an assumed height of 425 km. Swarm satellite data measured plasma parameters that showed strong subauroral ion drift signatures when the SAR arc was observed. These conditions intensified to extremely high values in a thinner channel when STEVE was present. Our results highlight the fast evolution of plasma properties and their effects on optical emissions. Current theories and models are unable to reproduce or explain these observations.

Plain Language Summary A variety of optical structures are observed in the "subauroral" region. This region is at lower latitudes adjacent to the auroral zone. These phenomena are distinct from auroras, as their optical signatures appear to be triggered by extreme thermal and kinetic energy in Earth's atmosphere, rather than produced by energetic particles raining down into our atmosphere. Two such subauroral optical structures are "stable auroral red (SAR) arcs" and "Strong Thermal Emission Velocity Enhancement (STEVE)". Although, SAR arcs and STEVE, both occur during geomagnetically active conditions in the subauroral region, their appearance differs significantly with distinct spectra, scale-size, and duration. We combined images captured by a citizen scientist in New Zealand on 17 March 2015 with data from a scientific all-sky imager as well as satellites. We observed the evolution of an unusually bright SAR arc into STEVE. We show satellite measurements of a region of fast-moving particles, known as "subauroral ion drift," at the same time the SAR arc occurred. Later, when STEVE was present, these conditions further intensified into a narrower band with higher temperature and faster flows. These observations highlight the benefits of combining citizen scientist observations with scientific data to help discover new connections in Geospace.

1. Introduction

The subauroral upper atmosphere is located equatorward of the auroral oval and presents a wide variety of magnetosphere-ionosphere-thermosphere processes. While connections between some of the processes that occur in this region have been identified, a connection has not been established for several phenomena. Perhaps, the most well-known optical structure observed in the subauroral region since the late 50s is an east-west elongated monochromatic long-lived arc, named stable auroral red (SAR) arc (Barbier, 1960; Kozyra et al., 1997), with typically dim brightness of ~500 R (Baumgardner et al., 2007). Associated with it, strong westward plasma flows, known as subauroral polarization streams (SAPS) or Subauroral Ion Drift (SAID) have been measured (Foster & Burke, 2002; Foster et al., 1994). The accepted SAR arc generation mechanism involves heat conduction from the inner magnetosphere into the subauroral region where the ionospheric trough is found (Cole, 1965; Kozyra et al., 1997). This energy flow into low plasma density results in high electron temperature, a typical configuration that produces local excitation of atomic oxygen, the main neutral constituent, and a consequent emission of 630.0 nm photons.

More recently, another type of east-west elongated subauroral arc was discovered by citizen scientists and named Strong Thermal Emission Velocity Enhancement (STEVE) (MacDonald et al., 2018). The source of this structure and the conditions conducive to its occurrence are still not well understood (Gallardo-Lacourt, Liang, et al., 2018). The first studies reported the presence of extreme conditions, corresponding to intense SAID, ≥∼2 km/s, and auroral substorms, as necessary for STEVE occurrence (Archer, Gallardo-Lacourt, et al., 2019; Gallardo-Lacourt, Nishimura, et al., 2018; MacDonald et al., 2018; Nishimura et al., 2019). In contrast to the monochromaticity of SAR arcs, spectrographic measurements of STEVE revealed multi-wavelegth emissions and relatively uniform emission across the visible spectrum (Gillies et al., 2019). A plausible generation mechanism involves the excitation of nitrogen molecules by fast-moving ions and subsequent broadband emission (Harding et al., 2020; Mende & Turner, 2019). This mechanism requires a minimum of ∼3 eV, equivalent to 4.4 km/s for NO^+ (the dominant ion in SAIDs), thus explaining why STEVE is observed during intense SAIDs. Some studies have shown that STEVEs and SAR arcs can occur simultaneously while observed at different geographic locations (Martinis et al., 2021) or that STEVE can merge with a preexisting SAR arc (Liang et al., 2019). However, available observations have never allowed the examination of whether a SAR arc can evolve into STEVE (or vice versa).

The present study provides the first direct detection of a bright wide red arc associated with a SAR arc, evolving into a thin mauve arc identified as STEVE. Plasma parameters measured by satellites reveal SAID conditions that intensify during the time the SAR arc evolves into STEVE, showing that this evolution represents an extreme transition occurring in the ionosphere.

2. Data and Discussion

On 17 March 2015 auroral activity was observed from Dunedin (45.95°S, 170.32°E), New Zealand. Equatorward of the main auroral display, a wide east-west elongated red arc, known as a SAR arc was observed. The red arc was unusually bright, enough to be observed with the naked eye. Such elevated brightness is uncommon for SAR arcs that tend to be subvisual (Baumgardner et al., 2007). During this event, photographs using an all-sky camera were taken between 22:22 and 23:16 New Zealand Summer Time (UTC + 13 hr). While sky conditions were in general good for auroral observations, patchy clouds appeared during brief periods of time not allowing for clear observations of the entire sky. The camera used was a Canon EOS 5D Mark III with an EF8-15 mm f/4L fisheye lens and it was not pointing straight up, but toward the south. Each image had an exposure time of 10 s and the time between images was 5 s Figure 1 (a) shows three photographs taken at 9:27 UT, 9:51 UT, and 10:02 UT. Images are shown with south at the bottom and west to the right. Three main features are summarized as follows: an early bright red arc, identified as a SAR arc, wider in the west (left column), a uniform thin white-purplish arc observed later, identified as STEVE (middle column), and green picket fence overlaid onto STEVE at the end of the arc lifetime (right column). These images represent the temporal evolution of three distinctive phenomena observed at subauroral latitudes. Panels (b, c, and d) of Figure 1 show the images decomposed in red, green, and blue color channels, respectively. At 09:27 UT, the red channel is the only one that shows a bright arc, without contributions from the green and blue channels. The bright emission to the south is diffuse aurora that appears in all channels. Interesting features are observed at this time. The western part of the arc seems to be brighter and wider and diffuse bright patches in the green channel lasting ∼10 min are observed to the west and south of the SAR arc (see Movie S1). In addition, a "dark" arc in the green channel is observed coinciding with the location of the red arc. It is unclear if this depleted emission can help to explain the subsequent changes that are observed. Similar reduced green line emissions have been reported during observations of STEVE (Yadav et al., 2021). The red-only contribution persists until ∼09:44 UT when the arc becomes uniformly narrower and starts to appear also in the green and blue channels (middle column). The contribution from the three channels is consistent with previous observations of STEVE events and it provides support for its multispectral nature (Gillies et al., 2019; Mende & Turner, 2019). Finally, the green picket fence structures observed at 10:02 UT (right column) are seen mainly in the green channel while the red channel detects a partial arc. The clear difference in the contributions of each color channel to the arc highlights its different nature at 09:27 UT and 09:51 UT. Supporting Information Movie S1 shows the entire sequence of observations.

The geomagnetic conditions on this night showed that the SAR arc occurred during the main phase of a geomagnetic storm. The transition into STEVE coincided with the recovery phase of a substorm (between ∼09:30 and ∼10:00 UT). Additional information is provided as Text S1 and Figure S1 in Supporting Information S1. A

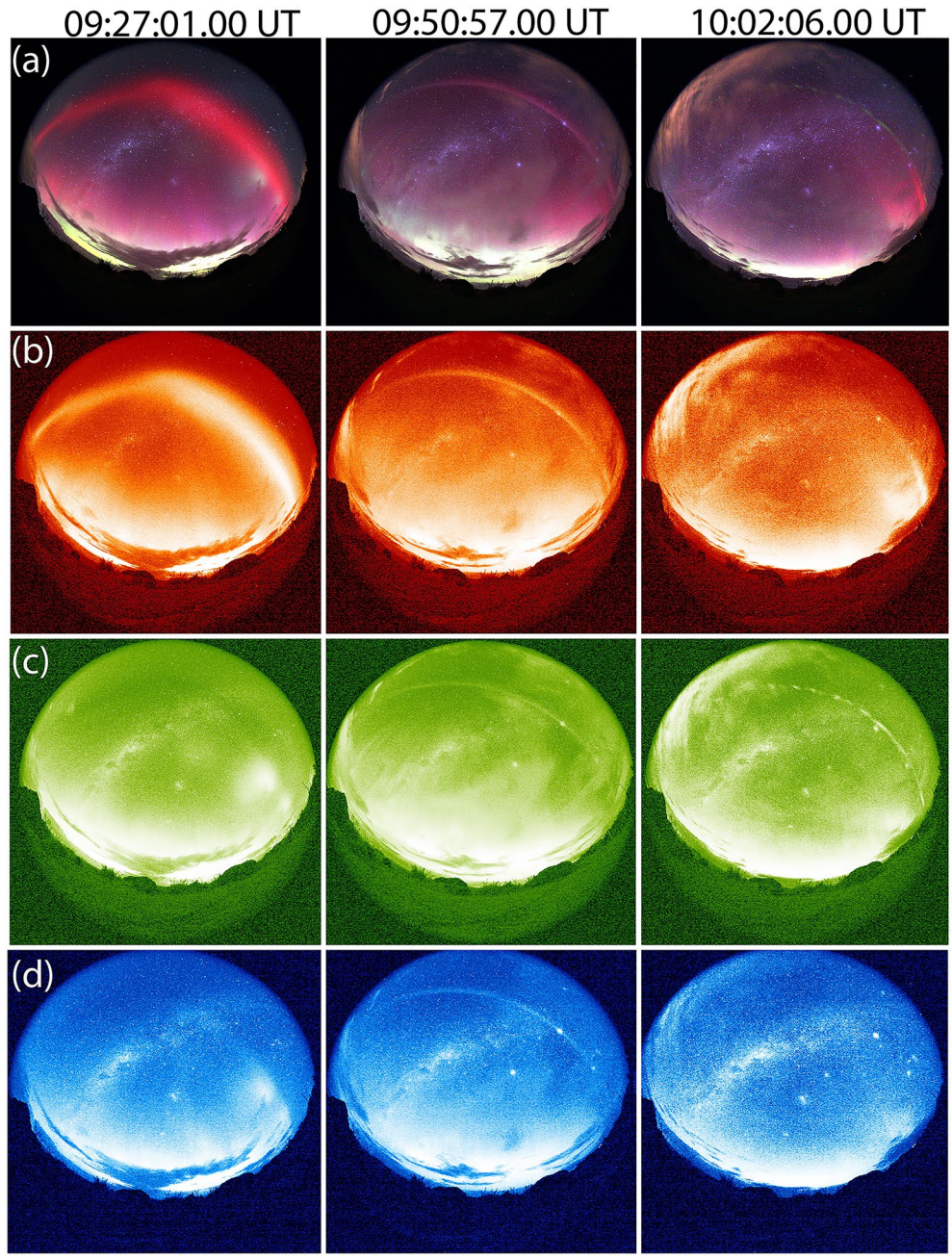

Figure 1. (a) A wide stable auroral red (SAR) arc is observed at 09:27 UT (left), a Strong Thermal Emission Velocity Enhancement (STEVE) at 09:51 UT (center), and a partial arc with green picket fence structures at 10:02 UT (right). Auroral activity is observed at the bottom (south) of each image. West is to the right; (b, c, and d) show decomposed images in red, green, and blue colors, respectively, at the same times as panel (a). At 09:27 UT (left) no arc is observed in the green and blue channels. At 09:51 UT (center), the three channels detect the arc. At 10:02 UT (right), the main emission comes from the green channel where picket fence structures are observed. A partial arc is also observed in the red channel to the right of the image.

timeline summarizing the observations from multiple sources and locations is shown in Figure S2 in Supporting Information S1.

Complementary data from an all-sky imager at the Mount John Observatory (43.99°S, 170.46°E), approximately 200 km north of Dunedin, part of the Boston University all-sky imager network (Martinis et al., 2018), provide key information on the initial stage of the observed SAR arc. Sky conditions over this site were cloudier than

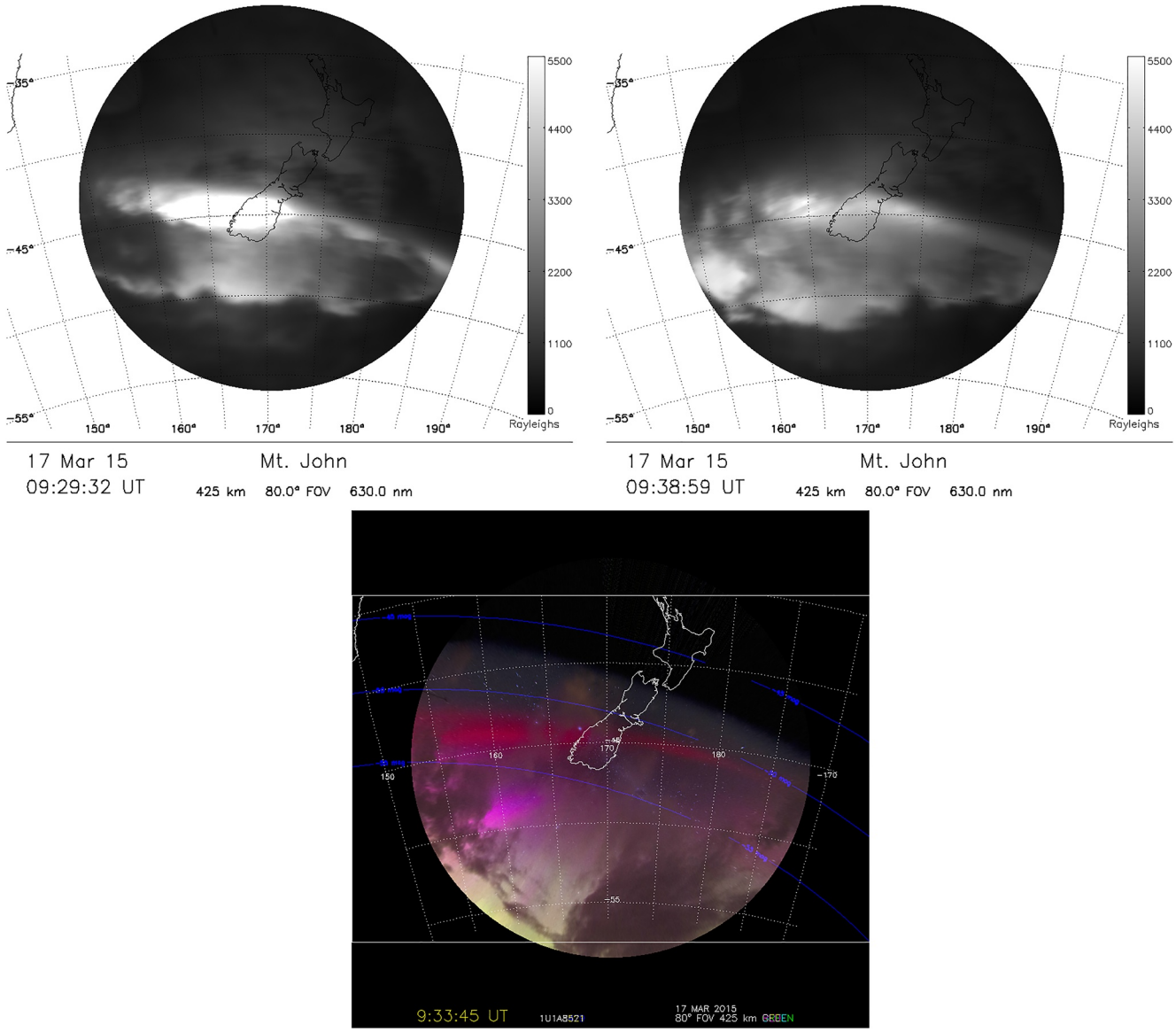

Figure 2. (top) Unwarped all-sky images from Mount John at 09:29 and 09:38 UT, using a height of 425 km and zenith angles down to 80°. Near zenith and to the east no clouds were present and the brightness of the stable auroral red arc at ∼45° latitude was ∼6 kR; (bottom) unwarped image from Dunedin at 09:33 UT, using the same parameters as in Mount John. Blue lines represent geomagnetic latitudes. The western edge of the arc is wider and brighter than the eastern edge.

at Dunedin and only a few frames allowed the observation of the arc close to zenith. Glimpses of an east-west elongated bright arc behind clouds were observed as early as ∼08:43 UT. The all-sky imager measures emissions in 630.0, 557.7, 589.3, and ≥695.0 nm. A filter centered at 520.7 nm is used to measure background emission for calibration purposes. The only wavelength that showed an arc-like structure was 630.0 nm, in agreement with the red-only arc observed from Dunedin.

In order to interpret the images and geolocate the structures observed, the data need to be processed and calibrated to assign geographic coordinates to each pixel (Baumgardner et al., 2007). An emission height of 425 km was chosen such that the arcs are seen from Mount John and Dunedin overlap. This height is in the range of typical altitudes of observed SAR arcs (Rees & Roble, 1975; Semeter & Mendillo, 1997). While a typical SAR arc brightness is ∼500 R (Baumgardner et al., 2007), the SAR arc observed on this night (after correcting vignetting and flat fielding effects) was at least 10 times brighter (∼6 kR) when measured on the locations not obstructed

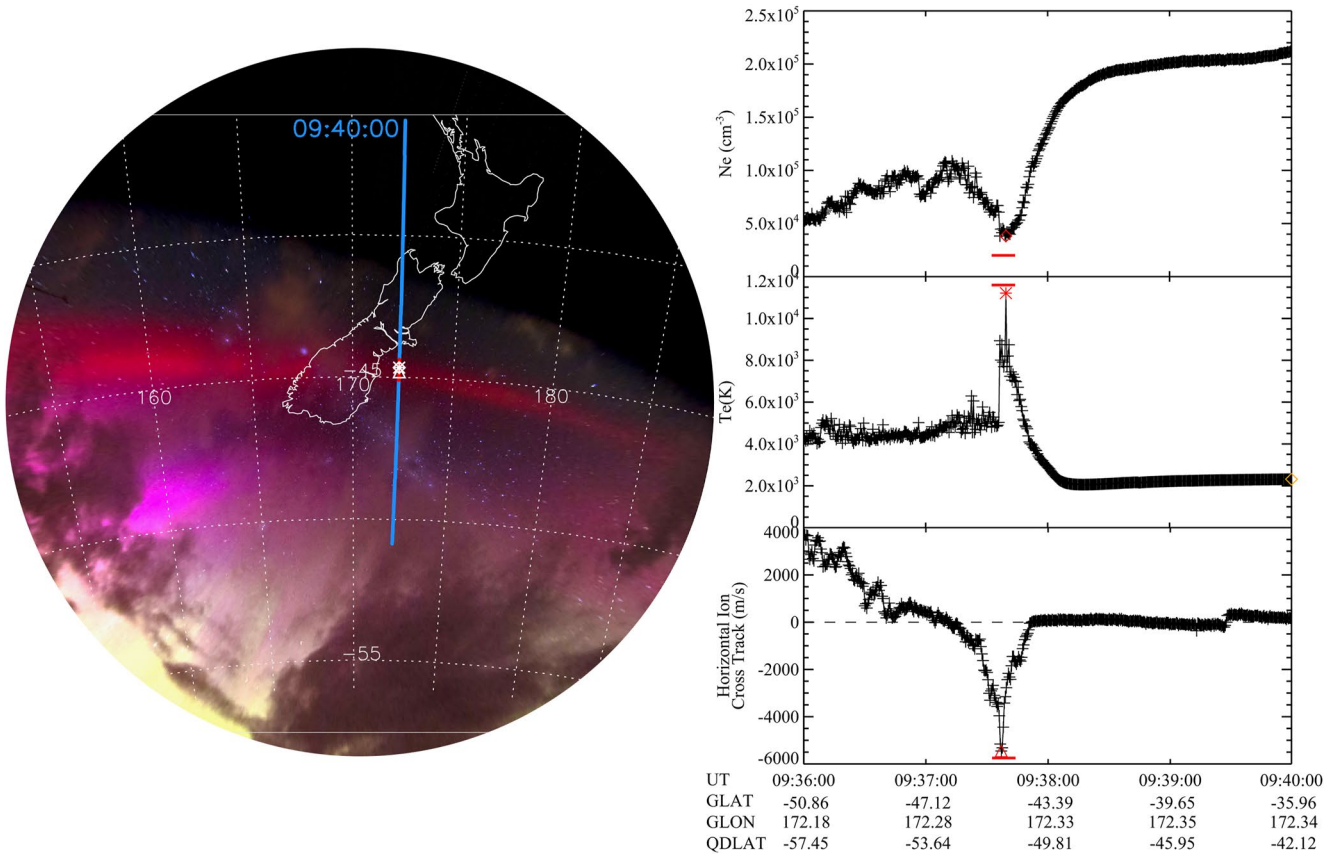

Figure 3. (left) Unwarped all-sky image from Dunedin assuming an emission height of 425 km. Swarm B trajectory is indicated as a blue line; (right) plasma parameters measured along the pass. From top to bottom: electron density (N_e), electron temperature (T_e), and horizontal plasma drift velocity (V_{hor}). N_e shows a small decrease coinciding with the stable auroral red arc location (horizontal red line). A colocated T_e enhancement is observed. V_{hor} shows a peak of ∼5.5 km/s. This peak seems to be a thin extension from a wider structure peaking at ∼3 km/s. Symbols indicating peaks in the plasma parameters were added in the plots and in the image to investigate their location on the arc.

by clouds. This unusually high brightness explains why the arc was visible to the citizen scientist in Dunedin. For reference, visible red aurora (measured in 630.0 nm) has a brightness of a few kR (Chamberlain, 1995).

Figure 2 shows at the top unwarped images from Mount John at 09:29 and 09:38 UT. The SAR arc is partially visible near zenith and to the east. Similar processing to geolocate the arc was applied to the citizen scientist data and the resulting image at 09:33 UT is shown at the bottom. The dark area at the top (north) corresponds to the edge of the field of view of the camera, and the beach/coastal area is at the bottom. The picture does not show the full sky because the camera was not pointing straight up but ∼35° off zenith to the south. Lines of constant magnetic latitude are drawn on the Dunedin image. The arc is not aligned with magnetic latitude lines, instead, its western edge is at a lower magnetic latitude than the eastern edge, a tilt observed in the past (Mendillo et al., 2016).

The latitudinal width of the SAR arc at 09:33 UT is around 1.0° in the Eastern portion of the image; while to the west is around 1.5–2.0°. This difference could be an indication of an ongoing evolution of an initially wider structure into a thin one. The three channels measured STEVE but with different widths, with the green arc thinner than the red arc (10:00 UT). At 10:04 UT, only a partial arc is visible to the west; this supports the idea of an asymmetric longitudinal evolution. Supporting Information Movies S2, S3, and S4 show unwarped movies in red, green, and blue channels, respectively.

During this event, data from Swarm B satellite were available. The satellite crossed the field of view of the optical instruments between 9:36 and 9:40 UT, moving northward at an altitude of 520 km in a quasi-polar orbit. The left panel in Figure 3 shows the image from Dunedin with the trajectory of Swarm B overlaid as a

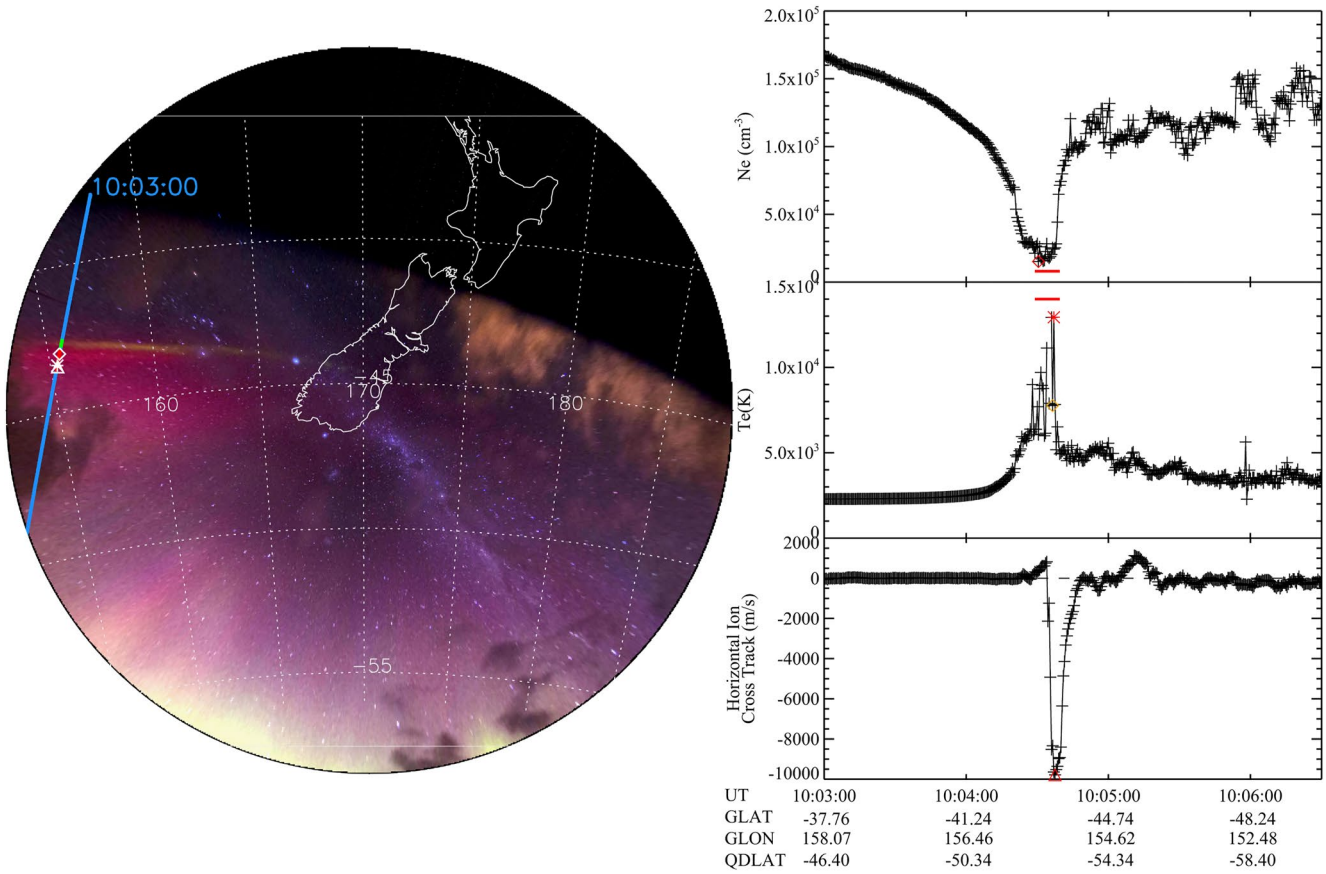

Figure 4. Similar to Figure 3 but with Swarm B trajectory in the Northern Hemisphere mapped to 425 km in the Southern Hemisphere. (left) Unwarped all-sky image from Dunedin. Symbols do not overlap exactly with the thin white-greenish arc, evidence of a lower emission height; (right) N_e decreases to ~1×10^4 cm^{-3} and T_e reaches ~10,000 K. V_{hor} increases to ~10 km/s and the plasma channel width is thinner.

blue line. The satellite trajectory was mapped to 425 km altitude along the Earth's magnetic field line using IGRF-12 (Thébault et al., 2015). The right panels in Figure 3 show, from top to bottom, plasma density (N_e), electron temperature (T_e), and horizontal plasma flow (V_{hor}) as a function of universal time, mapped geographic latitude, mapped geographic longitude, and magnetic latitude (QDLAT) (Richmond, 1995). N_e and T_e were obtained from the Langmuir probes on the electric field instrument, and V_{hor} was obtained from two thermal ion imager (TII) sensors (Knudsen et al., 2017). Of interest here are the reduced plasma density observed at ~45°S, reaching ~3×10^4 cm^{-3}, a collocated increase in T_e, that reaches 8000 K, and a strong westward plasma flow, V_{hor}, peaking at 5.5 km/s. This peak appears as a narrow spike within a wider structure (1.5–2° in latitude) that reaches ~2.5–3 km/s, a signature of a thin intense SAID embedded in a strong SAPS or wider SAID, a double structure previously reported (Foster & Burke, 2002; Grocott et al., 2011). The horizontal red line indicates the location of the arc along the mapped satellite trajectory. Symbols indicating peaks in the plasma parameters were added in each panel (diamond, asterisk, and triangle for Ne, Te, and V_{hor}, respectively) and in the image. The extremely large T_e and V_{hor} may help to explain the unusually high brightness measured with the all-sky imager and the visual detection by the citizen scientist. In addition to heat conduction from the inner magnetosphere (Mendillo & Wroten, 2019; Rees & Roble, 1975), frictional heating by the fast plasma flow could also contribute to the excitation of neutral species increasing airglow emission in 630.0 nm (Mishin & Streltsov, 2019; Sazykin et al., 2002).

The characteristics of the SAR arc described above clearly change after the Swarm B crossing. When the satellite reaches the Northern Hemisphere near the magnetic conjugate region of the Southern Hemisphere observations, at ~10:03 UT, the arc changes to a thin mauve-purplish structure. Figure 4 shows to the left, the Dunedin image with the mapped satellite trajectory (from the Northern Hemisphere at 520 km altitude to the Southern Hemisphere at

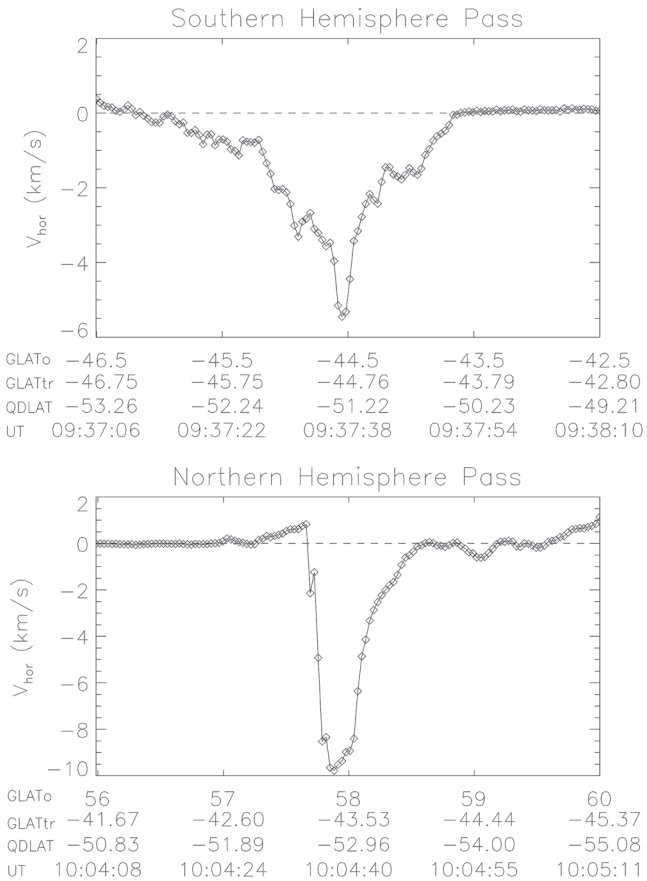

Figure 5. Horizontal velocity, V_{hor}, measured by Swarm B in the Southern Hemisphere (top) and in the Northern Hemisphere (bottom). $GLAT_o$, $GLAT_{tr}$, QDLAT, and UT represent the satellite latitude, satellite latitude mapped to 425 km, magnetic latitude at the mapped location, and universal time. The decrease in the width of the enhanced velocity is clearly observed in the Northern Hemisphere pass.

425 km). The plasma signatures are similar to the ones observed during the Southern Hemisphere pass, but now the changes are more pronounced, with N_e decreasing to 1×10^4 cm^{-3}, T_e reaching ∼10,000 K (with a couple of points exceeding this value), and V_{hor} peaking at ∼10 km/s. This velocity peak is now in a thinner channel as compared with the structure measured earlier. The symbols representing the peaks in N_e, T_e, and V_{hor} do not fall on top of the arc, which is evidence of a potential change in the height of the emission. A lower altitude emission might be more appropriate and consistent with a SAR arc that has evolved into STEVE, since the latter has been observed to occur at altitudes between ∼170 and 300 km (Archer, St.-Maurice, et al., 2019; Liang et al., 2019; Martinis et al., 2021) and not near 425 km.

Some T_e data points are flagged as not reliable in the data file, and negative values are also measured (not plotted). This could be of concern regarding the validity of the data. However, most of the measurements are reliable and show large values, highlighting the extreme conditions occurring in the region. The T_e measurements could be discarded if N_e is too low, but it is high enough (∼$1 - 3 \times 10^4$ cm^{-3}) to consider them as valid measurements. Instrument limitations to measure such high temperatures may affect some of the data. The TII sensors have not been tested nor calibrated for plasma drifts as large as ∼10 km/s. However, we can be confident that the flow velocity was significantly higher than the highest value of ∼6 km/s as previously reported (Archer, Gallardo Lacourt, et al., 2019). Current models and theories are not able to reproduce or explain T_e > ∼10,000 K or V_{hor} ∼10 km/s at subauroral ionospheric latitudes.

Additional information from Swarm-A and DMSP satellite data to the west of the optical measurements provide evidence of longitudinally perturbed plasma conditions, as well as extreme T_e that validate the Swarm-B data. Text S2 and Figures S3 and S4 in Supporting Information S1 provide details of the extreme conditions observed.

A closer examination of the latitudinal width of the enhanced plasma flow measured by Swarm B is shown in Figure 5. The initial width of the flow channel is around 1.5–2° with an embedded thinner feature ∼0.4° wide (top). Later, in the Northern Hemisphere, the width reduces to ∼0.6–0.7° (with no embedded thinner feature) (bottom). This is consistent with the optical observations recorded at the time, which show a thin and bright arc (∼0.3° in the green and ∼0.7° in the red channels). The peak velocities do not occur at the same magnetic latitude in both hemispheres. This is because the arc is not aligned along magnetic latitudes and the satellite samples, first the eastern part of the arc and then, in the Northern Hemisphere, the western part of the conjugate arc. We can hypothesize that, initially, Swarm B detected a wide and fast SAPS/SAID channel peaking at ∼3 km/s with an embedded thinner structure, resembling an intense SAID, that peaks at ∼6 km/s. Later, Swarm B measured a very fast and thin channel with apparent velocity V_{hor} that peaks as high as ∼10 km/s. This behavior seems consistent with the evolution of the wide SAR arc into a thin STEVE.

Several challenges can be found when studying intense subauroral phenomena such as STEVE/SAID events. For example, the Swarm observations are some of the best to study these intense events, but the plasma values are consistently beyond the expected range of measurements. Thus, future missions should consider instrumentation capable of measuring these extreme parameters. In addition, phenomena whose spectra evolve in time (SAR arc/STEVE transition) also highlight the need for high-quality spectral observations.

3. Conclusions

On 17 March 2015, citizen scientist images from Dunedin, New Zealand, show the evolution of a bright SAR arc into STEVE. The SAR arc was also measured by an all-sky imager at the Mount John Observatory, ∼200 km north of Dunedin. The SAR arc was unusually bright, reaching ∼6 kR. The SAR arc changed its width and emis-

sion characteristics by 09:45 UT and became a thin white-purplish structure, resembling a typical STEVE, with green picket fence structures also observed moving rapidly along the arc. The height of the initial arc was determined to be 425 km, but later a lower height seems more appropriate. Complementary information from Swarm B satellite data shows that the bright SAR arc was accompanied by large changes in the electron temperature and westward plasma flow. The plasma perturbations observed at the magnetic conjugate location of the optical observations were more extreme, with apparent values of V_{hor} reaching as high as 10 km/s and T_e ~10,000 K. Evidence from DMSP satellite data also points to an extended subauroral structure with plasma parameters changing between ~09:15 and 09:45 UT.

This work reports the first observation of a transition from a SAR arc into STEVE. This evolution is accompanied by a transition from an SAID into an extreme SAID in less than 30 min, with V_{hor} and T_e values exceeding previous measurements at subauroral latitudes. This result highlights the fast dynamics of the subauroral region and presents a challenge to theories and models of subauroral structures, their generation mechanisms, and how they relate to each other. This study shows the benefits of combining citizen scientist observations with scientific data to help discover new connections in Geospace.

Data Availability Statement

Swarm data are available from ESA at https://swarm-diss.eo.esa.int. The thermal ion imager data set used here is version 0302. The Langmuir probes data set used here is version 0502. Quick-look images and movies from the Boston University all-sky imager are available at http://sirius.bu.edu/data/?location=mt_john&year=2015&filt=6300&month=Mar&day=17. Unwarped and calibrated images can be found at https://doi.org/10.5281/zenodo.6462336. Raw multicolor Dunedin images are shown as a movie in Supporting Information S1 section. Processed images from individual RGB channels are available at https://doi.org/10.5281/zenodo.6520113. DMSP data were obtained from cdaweb.gsfc.nasa.gov as daily CDF and HDF files. RBSP-A data were downloaded from http://www.rbsp-ect.lanl.gov/rbsp_ect.php. Geomagnetic indices SYM-H and AL were obtained from the GSFC/SPDF OMNIWeb interface at https://omniweb.gsfc.nasa.gov. SML index was obtained from https://supermag.jhuapl.edu/.

Acknowledgments
This work was supported by National Science Foundation (NSF) Grant No. AGS-1552301 and AGS-2152365 (CM); NSF Grant Nos. AGS-1907698 and AGS-2100975 (YN); NASA Grant No. 80NSSC19K0286 (CM); NASA Grant Nos. NAS5-02099 and 80NSSC18K0657 (CM, YN); NASA Grant Nos. 80NSSC20K0604, 80NSSC20K0725, 80NSSC21K1321, and 80NSSC20K1788 (YN); NASA Postdoctoral Program (BG L); NASA Mesoscale ISFM (BGL); and Air Force Office Space Research Grant No. FA9559-16-1-0364 (YN). Swarm is a European Space Agency mission. Processing and calibration of the Thermal Ion Imager data are managed by J. Burchill at the University of Calgary under a grant from the Canadian Space Agency. The authors thank W.E. Archer for his careful review that has significantly improved the paper. C. Martinis thanks Jessica Norrell for her help in processing the Mount John all-sky images. C. Martinis thanks Dr. Juan Rodriguez-Zuluaga and Prof. Claudia Stolle for their inputs and discussions on availability and quality of Swarm data. B. Gallardo-Lacourt thanks Dr. Victor Pinto-Abarzua for useful discussions. C. Martinis thanks the Director and personnel from the Mount John Observatory for their continuing support of the Boston University all-sky imager.

References

Archer, W. E., Gallardo-Lacourt, B., Perry, G. W., St-Maurice, J.-P., Buchert, S. C., & Donovan, E. F. (2019). STEVE: The optical signature of intense subauroral ion drifts. *Geophysical Research Letters*, *46*, 6279–6286. https://doi.org/10.1029/2019GL082687

Archer, W. E., St.-Maurice, J.-P., Gallardo-Lacourt, B., Perry, G. W., Cully, C. M., Donovan, E., et al. (2019). The vertical distribution of the optical emissions of a Steve and Picket Fence event. *Geophysical Research Letters*, *46*(19), 10719–10725. https://doi.org/10.1029/2019GL084473

Barbier, D. (1960). L'arc auroral stable. *Annales Geophysicae*, *16*, 544–549.

Baumgardner, J., Wroten, J., Semeter, J., Kozyra, J., Buonsanto, M., Erickson, P., & Mendillo, M. (2007). A very bright SAR arc: Implications for extreme magnetosphere-ionosphere coupling. *Annales Geophysicae*, *25*(12), 2593–2608. https://doi.org/10.5194/angeo-25-2593-2007

Chamberlain, J. W. (1995). *Physics of the aurora and airglow*. American Geophysicsl Union. https://doi.org/10.1029/SP041

Cole, K. D. (1965). Stable auroral red arc, sinks for energy of DST main phase. *Journal of Geophysical Research*, *70*(7), 1689–1706. https://doi.org/10.1029/jz070i007p01689

Foster, J. C., Buonsanto, M. J., Mendillo, M., Nottingham, D., Rich, F. J., & Denig, W. (1994). Coordinated stable auroral red arc observations: Relationship to plasma convection. *Journal of Geophysical Research*, *99*(A6), 11429–11439. https://doi.org/10.1029/93JA03140

Foster, J. C., & Burke, W. J. (2002). SAPS: A new categorization for sub-auroral electric fields. *Eos Trans. AGU*, *83*(36), 393–394. https://doi.org/10.1029/2002EO000289

Gallardo-Lacourt, B., Liang, J., Nishimura, Y., & Donovan, E. (2018). On the origin of STEVE: Particle precipitation or ionospheric skyglow? *Geophysical Research Letters*, *45*, 7968–7973. https://doi.org/10.1029/2018GL078509

Gallardo-Lacourt, B., Nishimura, Y., Donovan, E., Gillies, D. M., Perry, G. W., Archer, W. E., et al. (2018). A statistical analysis of STEVE. *Journal of Geophysical Research: Space Physics*, *123*, 9893–9905. https://doi.org/10.1029/2018JA025368

Gillies, D. M., Donovan, E., Hampton, D., Liang, J., Connors, M., Nishimura, Y., et al. (2019). First observations from the TREx spectrograph: The optical spectrum of STEVE and the picket fence phenomena. *Geophysical Research Letters*, *46*, 7207–7213. https://doi.org/10.1029/2019GL083272

Grocott, A., Milan, S. E., Baker, J. B. H., Freeman, M. P., Lester, M., & Yeoman, T. K. (2011). Dynamic subauroral ionospheric electric fields observed by the Falkland Islands radar during the course of a geomagnetic storm. *Journal of Geophysical Research*, *116*(A11), A11202. https://doi.org/10.1029/2011JA016763

Harding, B. J., Mende, S. B., Triplett, C. C., & Wu, Y.-J. J. (2020). A mechanism for the STEVE continuum emission. *Geophysical Research Letters*, *47*, e2020GL087102. https://doi.org/10.1029/2020GL087102

Knudsen, D. J., Burchill, J. K., Buchert, S. C., Eriksson, A. I., Gill, R., Wahlund, J.-E., et al. (2017). Thermal ion imagers and Langmuir probes in the Swarm electric field instruments. *Journal of Geophysical Research: Space Physics*, *122*(2), 2655–2673. https://doi.org/10.1002/2016JA022571

Kozyra, J. U., Nagy, A. F., & Slater, D. W. (1997). High-altitude energy source(s) for stable auroral red arcs. *Reviews of Geophysics*, *35*(2), 155–190. https://doi.org/10.1029/96rg03194

Liang, J., Donovan, E., Connors, M., Gillies, D., St-Maurice, J. P., Jackel, B., et al. (2019). Optical spectra and emission altitudes of double-layer STEVE: A case study. *Geophysical Research Letters*, *46*, 13630–13639. https://doi.org/10.1029/2019GL085639

MacDonald, E. A., Donovan, E., Nishimura, Y., Case, N. A., Gillies, D. M., Gallardo-lacourt, B., et al. (2018). New science in plain sight: Citizen scientists lead to the discovery of optical structure in the upper atmosphere. *Science Advances*, *4*(March), 16–21. https://doi.org/10.1126/sciadv.aaq0030

Martinis, C., Baumgardner, J., Wroten, J., & Mendillo, M. (2018). All-sky-imaging capabilities for ionospheric space weather research using geomagnetic conjugate point observing sites. *Advances in Space Research*, *61*(7), 1636–1651. https://doi.org/10.1016/j.asr.2017.07.021

Martinis, C., Nishimura, Y., Wroten, J., Bhatt, A., Dyer, A., Baumgardner, J., & Gallardo-Lacourt, B. (2021). First simultaneous observation of STEVE and SAR arc combining data from citizen scientists, 630.0 nm all-sky images, and satellites. *Geophysical Research Letters*, *48*(8), e2020GL092169. https://doi.org/10.1029/2020GL092169

Mende, S. B., & Turner, C. (2019). Color ratios of subauroral (STEVE) arcs. *Journal of Geophysical Research: Space Physics*, *124*(7), 5945–5955. https://doi.org/10.1029/2019ja026851

Mendillo, M., Baumgardner, J., & Wroten, J. (2016). SAR arcs we have seen: Evidence for variability in stable auroral red arcs. *Journal of Geophysical Research: Space Physics*, *121*(1), 245–262. https://doi.org/10.1002/2015ja021722

Mendillo, M., & Wroten, J. (2019). Modeling stable Auroral red (SAR) arcs at geomagnetic conjugate points: Implications for hemispheric asymmetries in heat fluxes. *Journal of Geophysical Research: Space Physics*, *124*(7), 6330–6342. https://doi.org/10.1029/2019ja026904

Mishin, E., & Streltsov, A. (2019). STEVE and the picket fence: Evidence of feedback-unstable magnetosphere-ionosphere interaction. *Geophysical Research Letters*, *46*(24), 14247–14255. https://doi.org/10.1029/2019gl085446

Nishimura, Y., Gallardo-Lacourt, B., Zou, Y., Mishin, E., Knudsen, D. J., Donovan, E. F., et al. (2019). Magnetospheric signatures of STEVE: Implications for the magnetospheric energy source and interhemispheric conjugacy. *Geophysical Research Letters*, *46*, 5637–5644. https://doi.org/10.1029/2019GL082460

Rees, M. H., & Roble, R. G. (1975). Observations and theory of the formation of stable auroral red arcs. *Reviews of Geophysics*, *13*(1), 201. https://doi.org/10.1029/rg013i001p00201

Richmond, A. D. (1995). Ionospheric electrodynamics using magnetic apex coordinates. *Journal of Geomagnetism and Geoelectricity*, *47*, 191–212. https://doi.org/10.5636/jgg.47.191

Sazykin, S., Fejer, B. G., Galperin, Y. I., Zinin, L. V., Grigoriev, S. A., & Mendillo, M. (2002). Polarization jet events and excitation of weak SAR arcs. *Geophysical Research Letters*, *29*(12), 1586. https://doi.org/10.1029/2001GL014388

Semeter, J., & Mendillo, M. (1997). A nonlinear optimization technique for ground-based atmospheric emission tomography. *IEEE Transactions on Geoscience and Remote Sensing*, *35*(5), 1105–1116. https://doi.org/10.1109/36.628779

Thébault, E., Finlay, C. C., Beggan, C. D., Alken, P., Aubert, J., Barrois, O., et al. (2015). International geomagnetic reference field: The 12th generation. *Earth Planets and Space*, *67*(1), 79. https://doi.org/10.1186/s40623-015-0228-9

Yadav, S., Shiokawa, K., Otsuka, Y., Connors, M., & St Maurice, J.-P. (2021). Multi-wavelength imaging observations of STEVE at Athabasca, Canada. *Journal of Geophysical Research: Space Physics*, *126*(2), e2020JA028622. https://doi.org/10.1029/2020ja028622

References From the Supporting Information

Gabrielse, C., Nishimura, Y., Lyons, L., Gallardo-Lacourt, B., Deng, Y., & Donovan, E. (2018). Statistical properties of mesoscale plasma flows in the nightside high-latitude ionosphere. *Journal of Geophysical Research: Space Physics*, *123*(8), 6798–6820. https://doi.org/10.1029/2018JA025440

Gallardo-Lacourt, B., Nishimura, Y., Lyons, L. R., Mishin, E. V., Ruohoniemi, J. M., Donovan, E. F., et al. (2017). Influence of auroral streamers on rapid evolution of ionospheric SAPS flows. *Journal of Geophysical Research: Space Physics*, *122*, 12406–12420. https://doi.org/10.1002/2017JA024198

Gjerloev, J. W. (2012). The SuperMAG data processing technique. *Journal of Geophysical Research*, *117*(A9), A09213. https://doi.org/10.1029/2012JA017683

Newell, P. T., & Gjerloev, J. W. (2011). Evaluation of SuperMAG auroral electrojet indices as indicators of substorms and auroral power. *Journal of Geophysical Research*, *116*(A12), A12211. https://doi.org/10.1029/2011JA016779

Sergeev, V. A., Liou, K., Newell, P. T., Ohtani, S.-I., Hairston, M. R., & Rich, F. (2004). Auroral streamers: Characteristics of associated precipitation, convection and field-aligned currents. *Annales Geophysicae*, *22*(2), 537–548. https://doi.org/10.5194/angeo-22-537-2004